Available online at www.sciencedirect.com
ScienceDirect
Atmospheric Environment 40 (2006) 6465–6476
ATMOSPHERIC ENVIRONMENT
www.elsevier.com/locate/atmosenv

Atmospheric aerosols during the 2003 heat wave in southeastern Spain II: Microphysical columnar properties and radiative forcing

H. Lyamani[a,b], F.J. Olmo[a,b], A. Alcántara[a,b], L. Alados-Arboledas[a,b,*]

[a]Departamento de Física Aplicada, Facultad de Ciencias, Universidad de Granada. Fuentenueva s/n. 18071, Granada. Spain
[b]Centro Andaluz de Medio Ambiente (CEAMA), Junta de Andalucía-Universidad de Granada, Avda. del Mediterraneo s/n, 18071 Granada, Spain

Received 19 October 2005; received in revised form 26 April 2006; accepted 27 April 2006

Abstract

The columnar properties of atmospheric aerosol (size distributions, single scattering albedo and asymmetry parameter) are investigated based on sun/sky photometer measurements obtained during August 2003 at Granada (37.18°N, 3.58°W, 680 m a.s.l.), southeastern Spain. Also, we compute and analyze the average aerosol radiative forcing under two different atmospheric situations that occurred during the heat wave event that affected Western Europe during first half of August 2003: intrusions of desert dust and episodes of European–Mediterranean (EUR–MED) air masses influence, both combined with the impact of the intense biomass burning due to the multiple forest fires that affected southern Europe during this period. Interpretation of the results obtained in these analyses has been done using key synoptic aspects evidenced in a previous paper. The results showed that during the heat wave episode and under the different air masses influence the fine particle concentration was more important than that obtained after this event. In the situation of EUR–MED influence the single scattering albedo decreased sharply with wavelength from 0.91 ± 0.02 at 440 nm to 0.83 ± 0.04 at 1020 nm. These values are similar to those obtained by other authors for urban-industrial particles and biomass burning aerosols. The single scattering albedo reported during the dust events (0.87 ± 0.02 at 670 nm) was lower than that obtained using AERONET data characterizing pure desert dust, and did not show the spectral variation indicated in the literature, indicating the possible combination of dust, urban-industrial particles and biomass burning aerosols. Estimates of the local direct aerosol radiative forcing in the 400–700 nm wavelength range were obtained both at ground level and at the top of atmosphere (TOA). The daily radiative forcing efficiencies at the surface ranged between -78.2 and $-73.4\,\mathrm{W\,m^{-2}}$ whereas they were between -19.4 and $-14.5\,\mathrm{W\,m^{-2}}$ at TOA. Aerosol radiative forcing efficiencies at the surface and TOA were slightly larger for EUR–MED case than for desert dust episode. Nevertheless, the daily atmospheric radiative forcing efficiencies obtained in the both cases were similar, about $59\,\mathrm{W\,m^{-2}}$, indicating that during desert dust episode dust was mixed with considerable amounts of absorbing aerosols.

Keywords: Aerosol properties; Radiative forcing; Saharan dust and forest fires

*Corresponding author. Departamento de Física Aplicada, Facultad de Ciencias, Universidad de Granada. Fuentenueva s/n. 18071, Granada. Spain. Tel.: +34 58 244024; fax: +34 58 243214.
E-mail address: alados@ugr.es (L. Alados-Arboledas).

1352-2310/$ - see front matter
doi:10.1016/j.atmosenv.2006.04.047

1. Introduction

Atmospheric aerosols are one of the most variable components of the Earth's atmospheric environment, and are known to influence the energy budget and climate. Atmospheric aerosols directly affect the radiation budget and climate by increasing atmospheric back-scattered radiation and by absorbing solar and long wave radiation (Haywood and Shine, 1997). Thus, in contrast to the greenhouse gases, which only cause warming, atmospheric aerosols—depending on their properties, especially single scattering albedo—can cause either cooling or warming of the atmosphere. Atmospheric aerosols also can indirectly affect the Earth's radiation balance and climate by changing the microphysical properties of clouds and their lifetimes (Rosenfeld, 2000; Kaufman et al., 2005), thereby modifying the precipitation regime. They play a major role in atmospheric chemistry and hence affect the concentration of other minor atmospheric constituents like ozone (Schwartz et al., 1995). Understanding the direct influence of atmospheric aerosols on radiative transfer in the atmosphere requires knowledge of their columnar optical and radiative properties, such as single scattering albedo and aerosol spectral optical depth (Haywood and Boucher, 2000). However, while the radiative forcing due to greenhouse gases is known with reasonably high degree of accuracy, uncertainties relating to aerosol radiative forcing remain very large (IPCC, 2001). This is due to the great spatial and temporal variability of atmospheric aerosols. There is significant variability of aerosol properties because of the great variability in the source of atmospheric aerosols, chemical compositions and lifetimes. There is also seasonal and interannual variability even if certain aerosol type dominates at one location because of different meteorological characteristics (Eck et al., 2001a).

Under special circumstances the regional aerosol load can undergo important increases. This can have large impact on the atmospheric aerosol properties and can lead to a large change of radiative fluxes at surface, free troposphere, and top of atmosphere (TOA). In a complementary paper (Lyamani et al., 2006; hereafter referred to as LY2006), we have shown that the intense heat wave that affected western Europe during first part of August 2003 is an example of this kind of situations.

In LY2006 the main features of the spectral aerosol optical depth at Granada in southeastern Spain were interpreted in light of back trajectory analysis and synoptic meteorological conditions. The observations showed that an exceptionally long lasting high turbidity event occurred at Granada area during first part of August 2003 coinciding with the exceptional heat wave that affected much of Europe (Lyamani et al., 2006). The characterization of this event represents a step to better understanding of atmospheric aerosol properties during severe heat waves, which are expected to become more intense and frequent in the future (IPCC, 2001).

In this paper, we address additional aspects on the atmospheric aerosol characterization during this heat wave event. Thus, we use the combination of aerosol optical depth measurements and sky radiance, obtained by means of an automatic radiometer CIMEL CE-318, to retrieve the columnar volume size distributions together with other properties of the atmospheric aerosol such as the single scattering albedo and asymmetry parameter. Interpretation of the results obtained in these analyses is done using key aspects evidenced in LY2006. Also, we address the evaluation of the atmospheric aerosol radiative forcing under two different situations that occurred during the heat wave period: intrusion of desert dust and episode of EUR–MED air masses influence, both combined with the influence of biomass burning emissions from multiple forest fires that affected southern Europe.

2. Experimental site and instrumentation

The data used in this study have been measured in August 2003 at the radiometric station of the University of Granada (37.18°N, 3.58°W, 680 m a.m.s.l), located in the rooftop of the Science Faculty building. Granada located in southeastern Spain is a non-industrialized, medium-sized city, situated in a natural basin surrounded by mountains. The study area is about 200 km away from the African continent and approximately 50 km away from the western Mediterranean basin. LY2006 presents a detailed description of the site.

The measurements described in the present study were acquired by the sun-photometer CE-318-4 (CIMEL Electronic, France). This instrument, which was incorporated to the AERONET network (Holben et al., 1998) in late 2004, made measurements of the direct sun and diffuse sky radiances within the spectral range 340–1020 nm and 440–1020 nm, respectively (Holben et al., 1998). The direct sun measurements are obtained at 340, 380, 440, 675, 870, 940, and 1020 nm (nominal wavelengths). These measurements are then used to compute aerosol optical depth at each wavelength except for the 940 nm channel. In LY2006 a description of the CIMEL measurements, calibration procedure and data treatment for the retrieval of aerosol optical depth ($\delta_a(\lambda)$) have been included.

The sky radiance almucantar measurements are acquired in four spectral channels at 440, 670, 870, and 1020 nm. For each solar zenith angle, sky radiances are taken at 28 azimuth angles within the relative angle range (from the sun) of 2–180° (Holben et al., 1998). We have calibrated the instrument for radiance measurements, at least twice a year, using an integrating sphere (Alados-Arboledas et al., 2004). In the following section we focus on the details concerning the retrieval of aerosol columnar properties by inversion of aerosol optical depth and sky radiance data.

3. Methodology

The sky radiance almucantar measurements at 440, 675, 870, and 1020 nm in conjunction with solar direct irradiance measurements at these same wavelengths, were utilized to retrieve the volume size distribution ($\mathrm{d}V(r)/\mathrm{d}\ln r$ ($\mathrm{cm^3\,cm^{-2}}$)), the single scattering albedo, $\omega_{0A(\lambda)}$, and the asymmetry parameter, g_λ, at these four wavelengths based on the method of Nakajima et al. (1996). In this method the refractive index is invariant with wavelength. The aerosol size distribution, single scattering albedo and asymmetry parameter are derived by iteration, minimizing the residuals between measured and calculated radiances (Alados-Arboledas et al., 2004; Kim et al., 2004; Olmo et al., 2006). The real part of the complex aerosol refractive index used in the iterative process is varied in the range 1.33–1.55 by 0.02 steps, while the imaginary part is set to zero. Then the optimal real part of refractive index obtained by the iterative process is fixed and imaginary part is varied in the range 0–0.01 by 0.0005 steps. The solution of the iterative process would be a columnar size distribution, single scattering albedo, asymmetry parameter and optimal refractive index for which the residuals between measured and calculated radiances are minimal.

The difference between measured almucantar radiances from both sides of the Sun (symmetry) was used as a check for the homogeneity of the sky conditions during the measurement process, discarding asymmetrical situations (root mean square deviation—RMSD—$>$10%) associated with inhomogeneous atmospheric conditions or the presence of clouds. The almucantar measurements that fulfil these requirements were used as input in the retrieval algorithm, and then the calculated radiances obtained using the retrieved aerosol parameters were compared against the measured values. Retrievals are discarded if the RMSD between observed and calculated radiance is greater than 7% in an absolute sense.

Moreover, the algorithm used is based on a spherical particles assumption. However, for the accurate retrieval of aerosol properties from sky radiance measurements affected by mineral dust it is important to consider the influences of nonspherical particles, because retrieved results considering spherical particles seem to show unrealistic spectral dependence in the real part of the refractive index and artificially increased fine particle mode (Dubovik et al., 2000, 2002a). The retrieved phase function can also exhibit significant differences when spherical particles are assumed, but not to a degree to significantly alter single scattering albedo (Dubovik et al., 2000, 2002a). By contrast, the aerosol size distributions obtained by the method of Nakajima et al. (1996) do not show such artificially increased fine mode (Kim et al., 2004; Olmo et al., 2006). The uncertainty test made by Kim et al. (2005) on the Nakajima et al. (1996) method shows that the errors in the dust size distribution in the radius range 0.1–10 μm reach 18%. However, no significant shifts in the positions of mode radii or changes in the shape of size distributions are expected. Nonetheless influences of nonsphericity are better to be incorporated for improving the retrieval qualities in particular for large dust particles. For the retrieval of the size distributions we use the whole range of available scattering angles in each experimental case. By the way Kim et al. (2005) show that the single scattering albedo can be retrieved with reasonable high accuracy for high aerosol loading and large solar zenith angles Thus we retrieved the single scattering albedo and asymmetry parameter only for high aerosol loading, $\delta_a(440\,\mathrm{nm}) > 0.4$, and solar zenith angle $>50°$ (i.e., the range of scattering angle in measured solar almucantar $>100°$).

Radiative forcing is defined as the instantaneous increase/decrease of the net radiation due to an instantaneous change of a substance of radiative importance in the atmosphere such as aerosols, clouds, greenhouse gases, or others (i.e., Horvath et al., 2002). Most interesting are the radiative forcing at the TOA, at the surface and atmosphere. At the surface we define the aerosol radiative forcing as the downward flux computed for a given aerosol load minus that computed without aerosol. The TOA aerosol radiative forcing is defined as the upward flux computed without aerosol minus that calculated for the given aerosol load. The atmospheric radiative forcing is defined as the radiative forcing at TOA minus that at the surface Thus, in this study we have chosen the atmosphere free of aerosols as the reference case.

To carry out the radiative forcing computations we have used the radiative transfer computer code SBDART (Ricchiazzi et al., 1998), which is a discrete ordinates radiative transfer model (Stamnes et al., 1988). This algorithm includes multiple scattering in a vertically inhomogeneous nonisothermal plane-parallel media, and it has been shown to be computationally efficient and to reliably resolve the radiative transfer equation. This radiative transfer computer code characterizes aerosols using as input the solar zenith angle, the spectral aerosol optical depth, the spectral single scattering albedo, and the spectral asymmetry parameter. Other parameters used by the code are the spectral solar radiation, surface height, total ozone columnar concentration, surface albedo (fixed to 0.15 for our study area), the model atmosphere (in our case midlatitude with seasonal dependence), and the stratospheric aerosol (not assumed in our case). The output parameters of the code are the downward and the upward flux per wavelength interval at surface and at TOA. Calculations were performed and integrated over the 400–700 nm spectral range for solar zenith angles varying from 20° to 80°. The values of aerosol radiative forcing obtained at the different solar zenith angles are instantaneous values. Assuming that the aerosol optical depth does not change during the day and integrating over all positions of the sun we estimated the daily average aerosol forcing.

4. Results and discussion

4.1. Aerosol columnar size distributions

The retrieved aerosol size distributions were grouped according to the classification by air mass origins analyzed in LY2006. The distributions presented are effective total atmospheric column integrated size distributions that are consistent with the column integrated radiative effects of the aerosols. Within each air masses class the shape of the retrieved aerosol size distributions and position of the radius mode did not experience any significant changes. This result is in agreement with that obtained by Omar et al. (2005) who show that the intensive size distribution properties (mean radius and standard deviation) are relatively constant within each aerosol group. This fact led us to calculate the average size distribution corresponding to each class. The average aerosol size distributions obtained for classes labelled dust event (DE), EUR–MED and Atlantic (ATL) are presented in Fig. 1.

Under the desert dust influence we obtained bimodal size distributions with fine particle mode ($r<0.5\,\mu m$) found at 0.13–0.16 μm and coarse particle mode ($r>0.5\,\mu m$) at 1.5–2.5 μm. In the rest

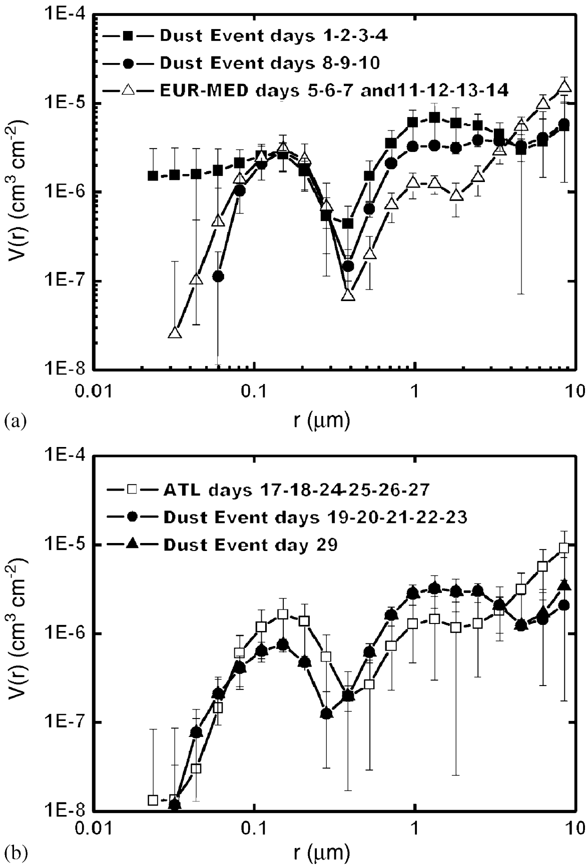

Fig. 1. Averaged aerosol size distributions grouped by air mass origin: (a) under heat wave conditions and (b) after the heat wave episode. DE: Dust Event, EUR–MED: European and Mediterranean influence and ATL: Atlantic influence.

of the cases three modes were evident, with the fine particle mode located at 0.13–0.16 μm, the first coarse mode at about 1 μm and the second coarse mode not well defined. During the heat wave episode, from 1 to 15 August 2003, the size distributions obtained under desert dust influence presented a marked mode for radius above 0.5 μm while the fine mode was also rather important (Fig. 1a). This situation is rather different from that associated with DEs that affected the area during the second half of August (Fig. 1b). In these last cases the coarse particle mode ($r > 0.5$ μm) more clearly dominated the volume size distribution. This was the consequence of the reduced contribution of fine particles long-range transported from Central and Eastern Europe and reduction in biomass burning emissions from Iberian peninsula and the change in the synoptic situation during the second part of August that does not favor the accumulation of fine particles (Lyamani et al., 2006). The fine mode radius does not show any significant change and is centred at ~0.15 μm. We obtained good agreement with the fine mode radius values (0.14–0.16 μm) reported for urban-industrial and biomass burning aerosols (Dubovik et al., 2002b; Omar et al., 2005).

In the EUR–MED cases the influence of the fine particles mode ($r < 0.5$ μm) is evident with a marked reduction in coarse particles (Fig. 1a). In any case during the heat wave episode and under the influence of different air masses the aerosol concentration associated with the fine particle mode, $r < 0.5$ μm, was more important than that obtained after this event. This increase in the fine particle contribution during the heat wave can be clearly observed in Fig. 2. In this figure, we show the evolution of fine particle concentration (V_F) calculated from the retrieved aerosol size distributions as suggested by Dubovik et al. (2002b). We can observe that V_F values obtained during the heat wave period were notably larger than those obtained after this event. During the heat wave period V_F was in the range 0.016–0.095 $\mu m^3\,\mu m^{-2}$ with an average value of $0.035 \pm 0.015\,\mu m^3\,\mu m^{-2}$, while after this event it was drastically reduced to between 0.005 and 0.029 $\mu m^3\,\mu m^{-2}$, with an average value of $0.014 \pm 0.006\,\mu m^3\,\mu m^{-2}$. This increment in the fine particle concentration during the heat wave period is due to a combination of circumstances. During this special event the contribution of biomass burning and EUR–MED influence combined with strong anticyclonic conditions (Lyamani et al., 2006) to reduce entrainment from the free troposphere and favor the accumulation of fine particles.

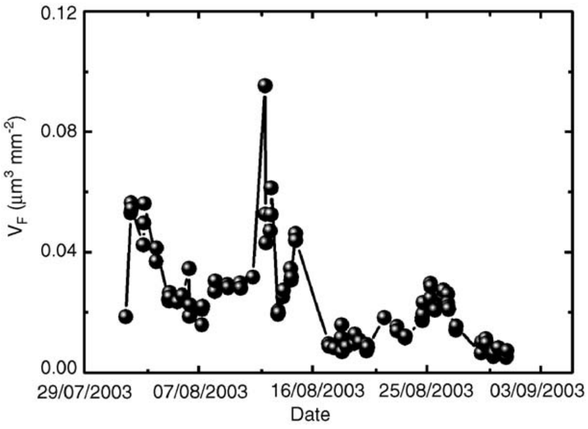

Fig. 2. Temporal evolution of aerosol concentration associated with the fine mode ($r < 0.5$ μm).

4.2. Single scattering albedo and asymmetry parameter

The single scattering albedo and the asymmetry parameter are key parameters for the estimation of the direct radiative impact of aerosols. The single scattering albedo is defined as the ratio of the scattering coefficient and the extinction coefficient. It depends on the relative source strengths of the various aerosol substances and on aging during transport. Absorption of solar radiation by atmospheric aerosols results mainly from elemental carbon originating from biomass burning and fuel combustion, and from mineral dust. The asymmetry parameter gives an indication of the angular distribution of the scattered radiation.

Table 1 presents the daily average values and corresponding standard deviations of $\omega_{0A(\lambda)}$ at the considered wavelengths during August 2003. Each average has been computed over a minimum of four experimental cases distributed between morning and afternoon. As an additional column we included the classification by air masses origin analyzed in LY2006. The values of $\omega_{0A(\lambda)}$ reveal the importance of aerosol absorption during the heat wave event.

During the dust outbreaks the $\omega_{0A(\lambda)}$ values are lower than those obtained by other authors for desert dust (Kaufman et al., 2001; Tanré et al., 2001; Dubovik et al., 2002b). These authors have obtained values of ω_{0A} (670 nm) in the range 0.95–0.99 for

Table 1
Daily average values and corresponding standard deviations of single scattering albedo

Day	ω_{0A} (440 nm)	ω_{0A} (670 nm)	ω_{0A} (870 nm)	ω_{0A} (1020 nm)	Classification by air mass origin
01/08/03	0.87 ± 0.01	0.86 ± 0.02	0.86 ± 0.02	0.87 ± 0.01	Dust event
02/08/03	0.89 ± 0.02	0.87 ± 0.02	0.87 ± 0.02	0.88 ± 0.02	Dust event
03/08/03	0.88 ± 0.02	0.85 ± 0.02	0.86 ± 0.02	0.87 ± 0.02	Dust event
08/08/03	0.90 ± 0.01	0.87 ± 0.01	0.86 ± 0.01	0.86 ± 0.01	Dust event
09/08/03	0.90 ± 0.01	0.87 ± 0.01	0.86 ± 0.01	0.87 ± 0.01	Dust event
10/08/03	0.91 ± 0.01	0.88 ± 0.01	0.87 ± 0.01	0.87 ± 0.01	Dust event
12/08/03	0.91 ± 0.02	0.87 ± 0.03	0.84 ± 0.03	0.83 ± 0.03	EUR–MED
14/08/03	0.92 ± 0.02	0.88 ± 0.03	0.85 ± 0.03	0.84 ± 0.03	EUR–MED

As an additional column we included the classification by air mass origin done in LY2006.

situations representative of pure desert dust. On the other hand, Perrone et al. (2005), using AERONET measurements made at Lecce (southern Italy) during situations affected by both Saharan dust and central Mediterranean anthropogenic aerosols, have obtained values of ω_{0A}(440 nm) ranging from 0.85 to 0.9. The results of these last authors agree well with the values of ω_{0A} (440 nm) in the range 0.87–0.91 obtained in this work during dust outbreaks that occurred during the heat wave.

Also, we have found a good agreement between our results corresponding to EUR–MED influence and those obtained during anthropogenic contamination influence as described by Eck et al. (2001b), Xia et al. (2005) and Mallet et al. (2003). Using measurements made at the Maldives during the INDOEX experiment, Eck et al. (2001b) found values of $\omega_{0A(\lambda)}$ decreasing from 0.91 at 440 nm to 0.83 at 1020 nm. In Beijing, China, Xia et al. (2005) using AERONET data have obtained $\omega_{0A(\lambda)}$ values of 0.89 at 440 nm and 0.84 at 1020 nm. Mallet et al. (2003), using AERONET measurements made during the ESCOMPTE experiment at a semi-urban site, Vallon Dol, south of France, have obtained an average value of ω_{0A} (550 nm) $= 0.86 \pm 0.05$. Also our values of $\omega_{0A(\lambda)}$ for EUR–MED influence are similar to those obtained at Mexico City and the Maldives for urban-industrial aerosols and at Cerrado, Brazil, for biomass burning aerosols (Dubovik et al., 2002b).

As we can observe, the aerosol present over our study area during the heat wave episode absorb almost as strongly as the aerosol over Mexico, Beijing, the Maldives and Cerrado. This high aerosol absorption is probably due to the presence of significant amounts of soot particles. In this sense, Satheesh et al. (1999) have shown that the soot particles, at the Maldives, contribute around 11% to the aerosol optical depth at 500 nm. Mallet et al. (2003) have determined that 90% of solar radiation extinction is due to anthropogenic aerosols, with 40% due to carbonaceous particles (20% is due to black carbon). Due to the high number of diesel vehicles and the great industrial activities in Mexico and Beijing an important presence of soot particles is expected. Also, the forest fires at Cerrado, Brazil, are expected to produce significant amounts of black carbon. Thus for our study area, in a small and non-industrialized city in comparison with Mexico and Beijing, the low presence of soot particles (high $\omega_{0A(\lambda)}$) is to be expected. The low values of $\omega_{0A(\lambda)}$ obtained at Granada during August 2003, similar to those obtained at areas with significant amounts of black carbon, indicate the potential effects of heat wave conditions on aerosol optical absorption properties. As commented in LY2006, during the heat wave episode the study area was under the influence of EUR–MED air masses and the effects of multiple intense forest fires that affected southern Europe and may have produced large contribution of soot particles. In addition, the anticyclonic conditions prevailing during the heat wave episode may have produced a large accumulation of this type of particle over the study area. Also, during this heat wave episode, the study area experienced frequent arrival of Saharan air masses which produced significant contribution of mineral dust, particles that are more absorbent in the ultraviolet and blue region (Claquin et al., 1999).

The spectral dependences of $\omega_{0A(\lambda)}$ obtained for DE and EUR–MED cases were appreciably different. In Fig. 3a we display the average values of $\omega_{0A(\lambda)}$ corresponding to DEs (1–3 and 8–10 August)

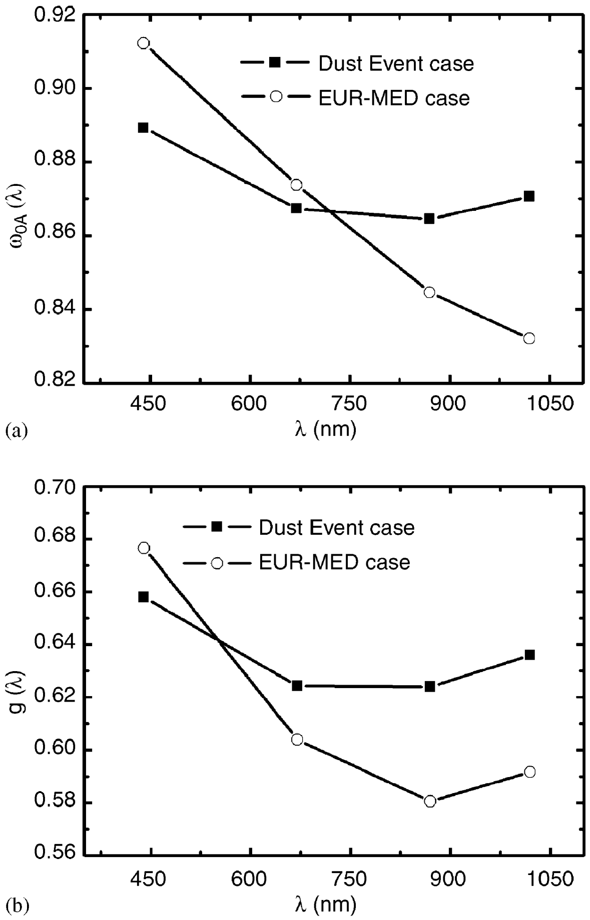

Fig. 3. Comparison between averaged values obtained during dust events (1–3 and 8–10 August) and European–Mediterranean influences (12 and 14 August) for: (a) single scattering albedo, (b) asymmetry parameter.

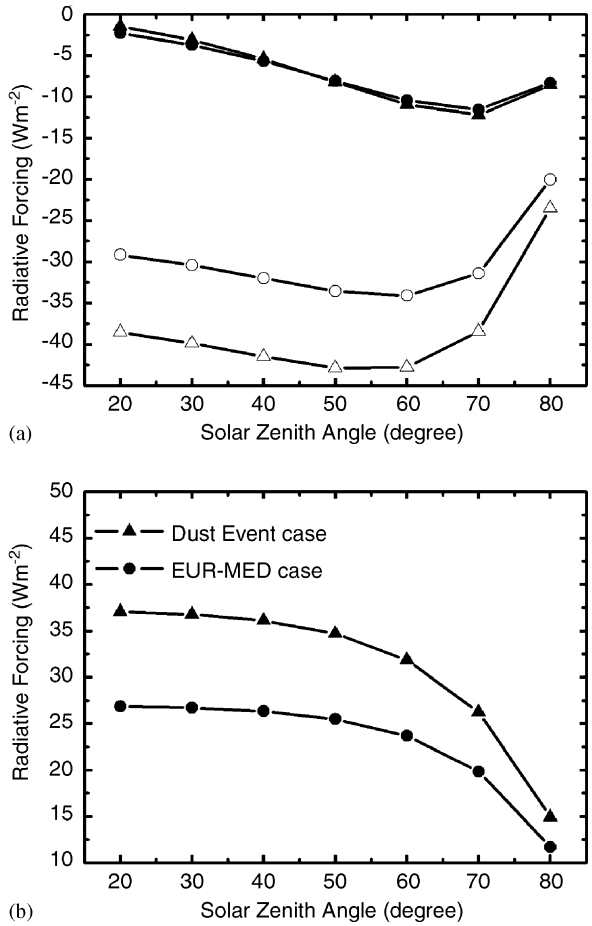

Fig. 4. (a) Radiative forcing at the surface (open symbols) and at TOA (full symbols) as function of solar zenith angle for dust events (1–3 and 8–10 August) (Δ) and European–Mediterranean cases (12 and 14 August) (○) and (b) atmospheric radiative forcing for the two cases studied here.

and EUR–MED cases (12 and 14 August). As can be seen, during EUR–MED influence the single scattering albedo decreased sharply with wavelength, according to the spectral variation characteristic of urban-industrial and biomass burning aerosols (Dubovik et al., 2002b; Eck et al., 2001a, b). The single scattering albedo during DEs case did not show the spectral variation (increasing with wavelength or the neutral dependency) indicated in the literature (Dubovik et al., 2002b; Collaud Coen et al., 2004). This difference with the literature results is due to the combination of dust, long-range transported urban-industrial particles and biomass burning aerosols during the DEs that occurred in our study area during heat wave period (Lyamani et al., 2006).

Daily average values of the asymmetry parameter obtained during the DEs—see Table 2—are lower than those obtained by Dubovik et al. (2002b) and Omar et al. (2005) for desert dust. Dubovik et al. (2002b), using AERONET measurements to characterize the desert dust, have obtained values of g(670 nm) around 0.66 ± 0.04 at Bahrain and Solar Ville, Saudi Arabia, and around 0.71 ± 0.04 at Cape Verde. Omar et al. (2005) have estimated an average value of g (673 nm) of 0.66 for the desert dust categories. AERONET measurements made at Creteil-Paris, France, and Mexico City to characterize the urban-industrial aerosols reveal that g_λ decreases from 0.68 at 440 nm to 0.57 at 1020 nm (Dubovik et al., 2002b). As we can observe, our results of g_λ for EUR–MED influence are similar to

Table 2
Daily average values and corresponding standard deviations of the asymmetry parameter

Day	g (440 nm)	g (670 nm)	g (870 nm)	g (1020 nm)	Classification by air mass origin
01/08/03	0.66 ± 0.02	0.64 ± 0.01	0.64 ± 0.02	0.65 ± 0.02	Dust event
02/08/03	0.64 ± 0.01	0.62 ± 0.01	0.63 ± 0.01	0.64 ± 0.01	Dust event
03/08/03	0.62 ± 0.02	0.62 ± 0.01	0.63 ± 0.01	0.65 ± 0.02	Dust event
08/08/03	0.68 ± 0.01	0.62 ± 0.02	0.61 ± 0.02	0.63 ± 0.02	Dust event
09/08/03	0.68 ± 0.01	0.62 ± 0.01	0.61 ± 0.01	0.63 ± 0.01	Dust event
10/08/03	0.68 ± 0.01	0.61 ± 0.01	0.60 ± 0.01	0.61 ± 0.01	Dust event
12/08/03	0.69 ± 0.01	0.60 ± 0.01	0.57 ± 0.01	0.58 ± 0.01	EUR–MED
14/08/03	0.66 ± 0.01	0.60 ± 0.01	0.58 ± 0.01	0.60 ± 0.02	EUR–MED

As an additional column we included the classification by air mass origin done in LY2006.

those obtained at Mexico City and Creteil-Paris and to those obtained by Omar et al. (2005) (g(673 nm) $\approx$ 0.61) for urban-industrial aerosols. The spectral dependences of g_{λ} corresponding to DEs (1–3 and 8–10 August) and to EUR–MED cases (12 and 14 August)—see Fig. 3b—were appreciably different. The asymmetry parameter at longer wavelength ($\lambda > 670$ nm) corresponding to DEs was greater than that corresponding to the EUR–MED case. This result indicates that at infrared wavelengths (670–1020 nm), for given aerosol optical depth, the solar radiation scattered to the surface was greater in the DEs case.

Table 3
Averaged values and standard deviations of single scattering albedo and asymmetry parameter representative of dust events (1–3 and 8–10 August) and European–Mediterranean influence (12 and 14 August)

Wavelength (nm)	EUR–MED influence ω_{0A} (λ)	EUR–MED influence g (λ)	Dust event ω_{0A} (λ)	Dust event g (λ)
440	0.91 ± 0.02	0.67 ± 0.02	0.89 ± 0.02	0.66 ± 0.02
670	0.87 ± 0.03	0.60 ± 0.01	0.87 ± 0.02	0.62 ± 0.01
870	0.84 ± 0.04	0.58 ± 0.01	0.86 ± 0.01	0.63 ± 0.02
1020	0.83 ± 0.04	0.59 ± 0.02	0.87 ± 0.01	0.64 ± 0.02

4.3. Radiative forcing

The important aerosol absorption and high aerosol load during the heat wave can produce a significant impact on aerosols radiative forcing (ARF) and significantly alter the radiative balance over the region. This would reduce the solar energy arriving at the surface, and thus produce significant surface cooling and atmospheric heating.

We calculated the ARF for DEs (1–3 and 8–10 August) and EUR–MED influence (12 and 14 August) cases using the spectral average values of $\omega_{0A(\lambda)}$ and g_{λ} given in Table 3 and corresponding averages values of $\delta_a(\lambda)$. The average value of δ_a(670 nm) was largest for DEs (0.28 ± 0.01) than for EUR–MED influence (0.20 ± 0.02).The average values of the Ångström exponent, α, were 0.88 and 1.47 for DEs and EUR–MED cases, respectively. The results are shown graphically in Fig. 4 as a function of the solar zenith angle. In the two cases studied here, the ARF is negative at both the surface and TOA indicating surface and TOA cooling in both cases. On the contrary, atmospheric ARF is positive in both cases indicating heating of the atmosphere.

At surface, the maximum radiative effect (in absolute sense) that occurred at solar zenith angle of 60° corresponds to a forcing about $-34.1\,\mathrm{W\,m^{-2}}$ for the EUR–MED case and $-42.9\,\mathrm{W\,m^{-2}}$ for DEs whereas at TOA the maximum radiative effect (in absolute sense) corresponds to a forcing of about $-12.0\,\mathrm{W\,m^{-2}}$ at 70° for both cases. As the solar zenith angle increases the ARF tends to increase (absolute value) both at TOA and at the surface up to 70° and 60°, respectively, due to the increase in photon path length and the associated increase in the attenuation, scattering and absorption, of direct solar radiation. For solar zenith angles greater than 60° the surface ARF decreased in absolute value with solar zenith angle in both cases. This can be explained by the long path at high solar zenith angle, which includes strong attenuation of direct solar radiation but also more multiple scattering and hence more scattered light. Also, for solar zenith angle greater than 70° the ARF at TOA decreased in absolute value with increasing solar zenith angle. In this case, part of the scattered light, even with predominant forward scattering, goes back to space.

Similar results were obtained by other authors. Using the same radiative transfer code utilized in this study to calculate the ARF, Horvath et al. (2002), using aerosol properties measurements made at Almeria (Spain) and Vienna (Austria) studied the ARF dependence on the solar zenith angle at the surface and TOA for surface albedo of 0.15 and 0.20. Their results showed that ARF at the surface has a maximum (in absolute value) at 50° for Almeria and at 60° for Vienna and that the negative ARF at TOA has a maximum (absolute value) at 70° for both sites. More recently, Meloni et al. (2005), using the aerosol optical properties measurements obtained at Lampedusa Island (Mediterranean Sea) showed that, during 2 days influenced by Saharan dust, the ARF (400–700 nm) at TOA had a maximum (absolute value) at 70° and that the ARF at surface had a maximum (absolute values) at 60–70°.

The daily average ARF is also estimated for the two cases studied here, assuming that the aerosol optical depth is constant during the day. The results are presented in Table 4. We also present the aerosol radiative forcing efficiency (ARFE), defined as the ARF divided by the aerosol optical depth at 670 nm, during the DE and EUR–MED influence cases. While the ARF is directly proportional to column aerosol amount represented by aerosol optical depth, the ARFE depends on the asymmetry parameter as well as the aerosol single scattering albedo. The daily average values are smaller than the instantaneous forcing due to the changes of solar zenith angle and the temporal integration that includes the night period. During DEs and EUR–MED cases the daily ARF at TOA was similar with values around $-4\,\mathrm{W\,m^{-2}}$, while the daily ARF for the surface and atmosphere were slightly greater (absolute value) during the DE case. The difference between the daily average ARF corresponding to the DEs case and EUR–MED influence around $4\,\mathrm{W\,m^{-2}}$ at the surface and at atmosphere can be taken as representative of the additional radiative forcing induced by dust aerosols. ARFE values during DE are expected to be much lower than those corresponding to anthropogenic contamination due to the weak absorption by dust particles (Tegen et al., 1996). However, the daily ARFE at the surface and TOA obtained for EUR–MED case were slightly greater (absolute values) than those calculated for DEs. Also, it is interesting to note the slight difference in the daily ARFE; in fact the atmospheric ARFE presented the same value for the two cases studied here. A possible explanation for this result is the strong influence of urban-industrial particles and biomass burning aerosols during the DEs analyzed in this study and the subsequent presence of considerable amounts of absorbing aerosols. In this sense we see that both EUR–MED and desert dust aerosols present similar values of single scattering albedo (in the visible range), but in the desert dust case the asymmetry parameter is slightly greater than that obtained for EUR–MED case. Thus, during the DE atmospheric aerosol scatter more solar radiation to the surface and less radiation to the space than during EUR–MED case. This could explain the slight differences in ARFE at TOA and surface, and coincidence in atmospheric ARFE. Taking into account the spectral interval difference, the daily average atmospheric ARF values obtained in this study are similar to those obtained at Lampedusa between 3 and 23 August 2003 by Pace et al. (2005). These authors calculated atmospheric ARF in 300–800 nm range assuming different aerosol vertical distributions. They estimated atmospheric ARF between 21.6 and $25.7\,\mathrm{W\,m^{-2}}$, where the lowest values is for the case of standard aerosol vertical distributions. The daily surface ARFE values obtained in this study are in the range values (from -54.0 to $-102.3\,\mathrm{W\,m^{-2}}$) obtained at the Mediterranean Island of Lampedusa by Meloni et al. (2003) for Saharan dust and aerosol originated from Europe. On the other hand, some differences are evident when we compare with the TOA daily

Table 4
Daily averaged radiative forcing and daily averaged radiative forcing efficiency of atmospheric aerosol during dust events (1–3 and 8–10 August) and European–Mediterranean cases (12 and 14 August)

		Dust event case	EUR–MED case
ARF ($\mathrm{W\,m^{-2}}$)	Surface	−20.4	−16.1
	TOA	−4.0	−4.0
	Atmosphere	16.4	12.1
ARFE ($\mathrm{W\,m^{-2}}/\delta_{670}$)	Surface	−73.4	−78.2
	TOA	−14.5	−19.4
	Atmosphere	58.9	58.8

ARF computed by these authors (Meloni et al., 2003). In fact they obtained values of $-3\,W\,m^{-2}$ for desert dust and close to zero or slightly positive for aerosol originating from Europe. This difference is due to the low single scattering albedo derived by these authors, which reveals the presence of more absorbing particles than in our case.

5. Summary

From 1 to 15 August 2003 a large part of Western Europe was affected by a severe heat wave (WHO, 2004). Using sun-photometric and sky radiance measurements from a CIMEL CE-318-4, atmospheric aerosol features (optical, physical and radiative properties) have been analyzed at Granada (Spain). During this special episode study area was alternatively influenced by Saharan and EUR–MED air masses, both combined with the influence of biomass burning from multiple forest fires that affected the southern Europe (Lyamani et al., 2006).

The size distributions obtained under dust influence were bimodal with a marked mode for radius above $0.5\,\mu m$ and a rather important submicron mode. This situation was different from that associated with DEs after the heat wave, when the coarse particle mode was clearly dominant. During EUR–MED influence fine particle concentrations were more important. In any case during the heat wave episode the fine particle concentration was more important than that obtained after this event, regardless of air mass origin.

During EUR–MED influence $\omega_{0A(\lambda)}$ decreased sharply with wavelength from 0.91 ± 0.02 at 440 nm to 0.83 ± 0.04 at 1020 nm whereas during DEs it did not show the spectral variation indicated in the literature. The values of $\omega_{0A(\lambda)}$ obtained under dust influences during the heat wave (0.87 ± 0.02 at 670 nm) are lower than those reported in the literature, indicating that the dust aerosols were also mixed with light-absorbing aerosols. The values of $\omega_{0A(\lambda)}$ obtained during EUR–MED influence are notably low and similar to those obtained by other authors in areas with high smoke and anthropogenic contamination levels. The asymmetry parameter at (670 nm) was 0.62 ± 0.01 and 0.60 ± 0.01 during DEs and EUR–MED influence, respectively.

Estimates of ARF in the 400–700 nm wavelength range were obtained both at ground level and TOA. The ARFE at the surface was slightly larger (absolute value) for aerosol of EUR–MED origin than for desert dust. However, the largest values of the aerosol optical depth are usually found in Saharan DEs, and the resulting surface ARF was larger. The additional daily average surface forcing induced by the desert dust was of about $4\,W\,m^{-2}$. The ARF at the TOA was negative, thus producing a similar cooling in both cases. This last result together with the similar daily atmospheric ARFE suggests the influence of urban-industrial particles and/or biomass burning aerosols during the DE.

These results represent features of the atmospheric aerosol properties and subsequent aerosol radiative forcing during heat wave episodes that—according to the IPCC—will be more frequent and of enhanced duration and intensity, especially in Europe and North America, in future global climate scenarios.

Acknowledgments

This work was supported by CICYT from the Spanish Ministry of Science and Technology through projects No: CGL2004-05984-C07-03 and REN2003-03175. The Spanish Meteorological Service kindly supplied the sun-photometer data. The ozone columnar contents were provided by INTA. Backward trajectories have been obtained by HYSPLIT4, available at the NOAA site http://www.arl.noaa.gov/ready/hysplit4.html, NOAA Air Resources Laboratory, Silver Spring, MD. We thank anonymous reviewers for their suggestion. We thank Dr. Kowalski who revised the English translation of the manuscript.

References

Alados-Arboledas, L., Olmo, F.J., Alcántara, A., Lyamani, H., Lorente, J., Martínez-Lozano, J.A., Cachorro, V., Labajo, A., de la Morena, B., Díaz, A., Pujadas, M., Horvath, H., Silva, A.M., Pavese, G., 2004. Veleta 2002 field campaign a general overview. Optica Pura y Aplicada 37 (3), 3271–3276.

Claquin, T., Schulz, M., Balkanski, Y.J., 1999. Modeling the mineralogy of atmospheric dust sources. Journal of Geophysical Research 104, 22243–22256.

Collaud Coen, M., Weingartner, E., Schaub, D., Hueglin, C., Corrigan, C., Henning, S., Schwikowski, M., Baltensperger, U., 2004. Saharan dust events at the Jungfraujoch: detection by wavelength dependence of the single scattering albedo and first climatology analysis. Atmospheric Chemistry and Physics 4, 1–16.

Dubovik, O., Smirnov, A., Holben, B.N., King, M.D., Kaufman, Y.J., Eck, T.F., Slutsker, I., 2000. Accuracy assessments of aerosol optical properties retrieved from Aerosol Robotic

Network (AERONET) Sun and sky radiance measurements. Journal of Geophysical Research 105 (D8), 9791–9806.
Dubovik, O., Holben, B.N., Lapyonok, T., Sinyuk, A., Mishchenko, M.I., Yang, P., Slutsker, I., 2002a. Non-spherical aerosol retrieval method employing light scattering by spheroids. Geophysical Research Letters 29, 10.
Dubovik, O., Holben, B., Eck, T.F., Smirnov, A., Kaufman, Y.J., King, M.D., Tanré, D., Slutsker, I., 2002b. Variability of absorption and optical properties of key aerosol types observed in worldwide locations. Journal of the Atmospheric Sciences 59 (3), 590–608.
Eck, T.F., Holben, B.N., Ward, D.E., Dubovik, O., Reid, J.S., Smirnov, A., Mukelabai, M.M., Hsu, N.C., O'Neill, N.T., Slutsker, I., 2001a. Characterization of the optical properties of biomass burning aerosols in Zambia during the 1997 ZIBBEE field campaign. Journal of Geophysical Research 106 (D4), 3425–3448.
Eck, T.F., Holben, B.N., Dubovik, O., Smirnov, A., Slutsker, I., Lobert, J.M., Ramanathan, V., 2001b. Column-integrated aerosol optical properties over the Maldives during the northeast monsoon for 1998–2000. Journal of Geophysical Research 106 (D22), 28555–28566.
Haywood, J.M, Boucher, O., 2000. Estimates of the direct and indirect radiative forcing due to tropospheric aerosols: a review. Reviews of Geophysics 38 (4), 513–543.
Haywood, J.M., Shine, K.P., 1997. Multi-spectral calculations of the direct radiative forcing of tropospheric sulphate and soot aerosols using a column model. Quarterly Journal of the Royal Meteorological Society-Part A 123 (543), 1907–1930.
Holben, B.N., Eck, T.F., Slutsker, I., Tanre, D., Buis, J.P., Setzer, A., Vermote, E., Reagan, J.A., Kaufman, Y.J., Nakajima, T., Lavenu, F., Jankowiak, I., Smirnov, A., 1998. AERONET—a federated instrument network and data archive for aerosol characterization. Remote Sensing of Environment 66 (1), 1–16.
Horvath, H., Alados-Arboledas, L.A., Olmo, F.J., Jovanovic, O., Gangl, M., Kaller, W., Sanchez, C., Sauerzopf, H., Seidl, S., 2002. Optical characteristics of the aerosol in Spain and Austria and its effect on radiative forcing. Journal of Geophysical Research-Atmospheres 107 (D19).
IPCC-Intergovernmental Panel on Climate Change, 2001. The Scientific Basis. Contribution of Working Group I to the Third Assessment report of the Intergovernmental Panel on Climate Change. Cambridge University Press, New York (p. 881).
Kaufman, Y.J., Tanre, D., Dubovik, O., Karnieli, A., Remer, L.A., 2001. Absorption of sunlight by dust as inferred from satellite and ground-based remote sensing. Geophysical Research Letters 28 (8), 1479–1482.
Kaufman, Y.J., Koren, I., Remer, L.A., Rosenfeld, D., Rudich, Y., 2005. The effect of smoke, dust, and pollution aerosol on shallow cloud development over the Atlantic Ocean. Proceedings of the National Academy of Sciences of the United States of America 102 (32), 11207–11212.
Kim, D.H., Sohn, B.J., Nakajima, T., Takamura, T., Takemura, T., Choi, B.C., Yoon, S.C., 2004. Aerosol optical properties over East Asia determined from ground-based sky radiation measurements. Journal of Geophysical Research 109, D02209.
Kim, D.H., Sohn, B.J., Nakajima, T., Takamura, T., 2005. Aerosol radiative forcing over East Asia determined from ground-based solar radiation measurements. Journal of Geophysical Research 110, D10S22.
Lyamani, H., Olmo, F.J., Alcantara, A., Alados-Arboledas, L., 2006. Atmospheric aerosols during the 2003 heat wave in southeastern Spain I: spectral optical depth. Atmospheric Environment, in press, doi:10.1016/j.atmosenv.2006.04.048.
Mallet, M., Roger, J.C., Despiau, S., Dubovik, O., Putaud, J.P., 2003. Microphysical and optical properties of aerosol particles in urban zone during ESCOMPTE. Atmospheric Research 69 (1–2), 73–97.
Meloni, D., di Sarra, A., DeLuisi, J., Di Iorio, T., Fiocco, G., Junkerman, W., Pace, G., 2003. Tropospheric aerosols in the Mediterranean:2. Radiative effects through model simulations and measurements. Journal of Geophysical Research 108 (D10).
Meloni, D., di Sarra, A., Di Iorio, T., Fiocco, G., 2005. Influence of the vertical profile of Saharan dust on the visible direct radiative forcing. Journal of Quantitative Spectroscopy & Radiative Transfer 93 (4), 397–413.
Nakajima, T., Tonna, G., Rao, R., Boi, P., Kaufman, Y., Holben, B., 1996. Use of sky brightness measurements from ground for remote sensing of particulate dispersion. Applied Optics 35, 2672–2686.
Olmo, F.J., Quirantes, A., Alcántara, A., Lyamani, H., Alados-Arboledas, L., 2006. Preliminary results of a non-spherical aerosol method for the retrieval of the atmospheric aerosol optical properties. Journal of Quantitative Spestroscopy & Radiative Transfer 100, 305–314.
Omar, A.H., Won, J.G., Winker, D.M., Yoon, S.C., Dubovik, O., McCormick, M.P., 2005. Development of global aerosol models using cluster analysis of Aerosol Robotic Network (AERONET) measurements. Journal of Geophysical Research 110 (D10), D10S14.
Pace, G., Meloni, D., di Sarra, A., 2005. Forest fire aerosol over Mediterranean basin during summer 2003. Journal of Geophysical Research 110, D21202.
Perrone, M.R., Santese, M., Tafuro, A.M., Holben, B.N., Smirnov, A., 2005. Aerosol load characterization over south-east Italy for one year of AERONET sun-photometer measurements. Atmospheric Research 75 (1–2), 111–133.
Ricchiazzi, P., Yang, S.R., Gautier, C., Sowle, D., 1998. SBDART: a research and teaching software tool for plane-parallell radiative transfer in the Earth's atmosphere. Bulletin of the American Meteorological Society 79 (10), 2101–2114.
Rosenfeld, D., 2000. Suppression of rain and snow by urban and industrial air pollution. Science 287, 1793–1796.
Satheesh, S.K., Ramanathan, V., Xu, L.J., Lobert, J.M., Podgorny, L.A., Prospero, J.M., Holben, B.N., Loeb, N.G., 1999. A model for the natural and anthropogenic aerosols over the tropical Indian Ocean derived from Indian Ocean Experiment data. Journal of Geophysical Research 104 (D22), 27421–27440.
Schwartz, S.E., Arnold, F., Blanchet, J.P., Durke, P.A., Hofmann, D.J., Hoppel, W.A., King, M.D., Lacis, A.A., Nakajima, T., Ogren, J.A., Toon, O.B., Wendisch, M., 1995. Group report: connections between aerosol properties and forcing of climate. In: Heintzenberg, J., Charlson, R.J. (Eds.), Aerosol of Climate. Wiley, New York, pp. 251–280.
Stamnes, k., Tsay, S.C., Wiscombe, W., Jayaweera, K., 1988. Numerically stable algorithm for discrete-ordinate-method radiative-transfer in multiple-scattering and emitting layered media. Applied Optics 27 (12), 2502–2509.

Tanré, D., Kaufman, Y.J., Holben, B.N., Chatenet, B., Karnieli, A., Lavenu, F., Blarel, L., Dubovik, O., Remer, L.A., Smirnov, A., 2001. Climatology of dust aerosol size distribution and optical properties derived from remotely sensed data in the solar spectrum. Journal of Geophysical Research 106, 18205–18217.

Tegen, I., Lacis, A.A., Fung, I., 1996. The influence on climate forcing of mineral aerosols from disturbed soils. Nature 380 (6573), 419–422.

Xia, X.A., Chen, H.B., Wang, P.C., Zong, X.M., Qiu, J.H., Gouloub, P., 2005. Aerosol properties and their spatial and temporal variations over North China in spring 2001. Tellus B 57 (1), 28–39.

WHO, 2004. Extreme weather and climate events and public health responses. Report on a WHO meeting Bratislava, Slovakia 09–10 February 2004. EUR/04/5036 794, World Health Organization, Regional Ofice for Europe, Geneva, pp. 15–24.